Journal of Power Sources 196 (2011) 5174–5185

Contents lists available at ScienceDirect

Journal of Power Sources

journal homepage: www.elsevier.com/locate/jpowsour

# Characterization of a zinc–cerium flow battery

P.K. Leung, C. Ponce-de-León*, C.T.J. Low, A.A. Shah, F.C. Walsh

*Electrochemical Engineering Laboratory, Energy Technology Research Group, University of Southampton, Highfield, Southampton, SO17 1BJ, United Kingdom*

ARTICLE INFO

*Article history:*
Received 26 November 2010
Accepted 25 January 2011
Available online 2 February 2011

*Keywords:*
Cerium
Energy storage
Methanesulfonic acid
Redox flow battery
Zinc

ABSTRACT

The performance of a divided, parallel-plate zinc–cerium redox flow battery using methanesulfonic acid electrolytes was studied. Eight two and three-dimensional electrodes were tested under both constant current density and constant cell voltage discharge. Carbon felt and the three-dimensional platinised titanium mesh electrodes exhibited superior performance over the 2-dimensional electrodes. The charge and discharge characteristics of the redox flow battery were studied under different operating conditions and Zn/Ce reactant, as well as methansulfonic acid concentration. The cell performance improved at higher operating temperatures and faster electrolyte flow velocities. The number of possible cycles increased at reduced states of charge. During 15 min charge/discharge per cycle experiment, 57 cycles were obtained and the zinc reaction was found to be the limiting process during long term operation.



## 1. Introduction

Large and medium scale energy storage technologies can be combined with conventional power generation sources such as fossil fuels and hydro-electricity [1,2]. Insufficient energy storage capacity can lead to problems, such as raised volatility and an increased burden on electricity distribution systems [3]. Since the 1970s, a number of redox flow batteries (RFBs), such as the iron–chromium [4,5], all vanadium [6–10], zinc–bromine [11], polysulfide–bromine [12,13] and soluble lead acid cells [14] have been developed. A typical application of RFBs is load-leveling, which consists of storing energy during off-peak hours and releasing it when the demand rises [3,15]. RFB technology can also be used in combination with renewable power sources, such as photovoltaic cells [16–18] and wind turbines [17,18]. Due to the rapid growth of renewable energy and more advanced power generating sources, increasing attention has been given to the development of more advanced, reliable and safer redox flow batteries.

The first zinc–cerium system was developed by Plurion Inc. (UK) [19,20]. Other systems using these couples include the zinc–chlorine [26–28], zinc–bromine [11,29], zinc–ferricyanide [30], zinc–air [31], vanadium–cerium [32] and zinc–cerium [19,20] cells. Both zinc [21] and cerium [22] are advantageous materials for energy storage due to the relatively large differences between their standard electrode potentials in aqueous media. This results in a system with a high thermodynamic open-circuit cell voltage of *c.a.* 2.4 V, and a large maximum energy density. This large potential difference necessitates the correct selection of materials and suppression of secondary reactions such as the hydrogen and oxygen evolution. At the negative electrode, the main electrode reactions are the electrodeposition and dissolution of zinc on a planar carbon/polyvinyl-ester composite material [19,20]:

$$Zn(CH_3SO_3)_2 + 2H^+ + 2e^- \underset{\text{Discharge}}{\overset{\text{Charge}}{\rightleftarrows}} Zn + 2CH_3SO_3H \quad (E^0 = -0.76\,\text{V}\ vs.\ \text{SHE}) \tag{1}$$

while hydrogen evolution can also take place on this electrode:

$$2H^+ + 2e^- \overset{\text{Charge}}{\longrightarrow} H_2 \quad (E^0 = 0\,\text{V}\ vs.\ \text{SHE}) \tag{2}$$

At the positive electrode, the primary reaction is the oxidation process of Ce(III) and the reduction of Ce(IV) during charge and discharge, respectively. The positive standard electrode potential lies between 1.28 and 1.72 V *vs.* Ag|AgCl, depending on the background electrolyte [23].

$$2Ce(CH_3SO_3)_3 + 2CH_3SO_3H \underset{\text{Discharge}}{\overset{\text{Charge}}{\rightleftarrows}} 2Ce(CH_3SO_3) + 2H^+ + 2e^- \tag{3}$$

While oxygen evolution can also take place:

$$H_2O \overset{\text{Charge}}{\longrightarrow} \frac{1}{2}O_2 + 2H^+ + 2e^- \quad (E^0 = 1.23\ \text{V}\ vs.\ \text{SHE}) \tag{4}$$

* Corresponding author at: School of Engineering Sciences, University of Southampton, University Road, Southampton, SO17 1BJ, United Kingdom.
Tel.: +44 23 8059 8931; fax: +44 23 8059 7051.
*E-mail address:* capla@soton.ac.uk (C. Ponce-de-León).

0378-7753/$ – see front matter © 2011 Elsevier B.V. All rights reserved.
doi:10.1016/j.jpowsour.2011.01.095

The overall cell reaction of the zinc–cerium redox flow battery, taking the standard potential of reaction (3) as 1.44 *vs.* SHE, is:

$$2Ce(CH_3SO_3)_3 + Zn(CH_3SO_3)_2 \underset{\text{Discharge}}{\overset{\text{Charge}}{\rightleftarrows}} Zn + Ce(CH_3SO_3)_4 \quad (E_{cell} = 2.4\ V) \tag{5}$$

Methanesulfonic acid is used as a solvent for both zinc and cerium ions, since its conductivity is comparable to that of hydrochloric acid, while posing a lower risk of corrosion compared with other mineral acids, such as sulphuric acid and is highly stable [24]. Cerium in methanesulfonic acid has the advantage of easy preparation and high solubility. The solubility limits of Ce(III) and Ce(IV) ions in methanesulfonic acid can be as high as 1 mol $dm^{-3}$, compared to less than 0.5 mol $dm^{-3}$ in sulphuric acid. The solubility of zinc is also high (2.16 mol $dm^{-3}$) in this acid [25].

Although previous work by Plurion Inc. has been described in several patents [19,20], information on the experimental conditions and discharge performance is limited. Moreover, few papers in the literature consider the use of zinc and cerium in aqueous methanesulfonic acid [25]. An improved understanding of the flow battery performance under various operating conditions and electrolyte compositions are crucial. In this work, a comprehensive investigation is carried out with regards to the optimal electrode materials and characterization of the zinc–cerium system.

## 2. Experimental details

### 2.1. Chemicals

Analytical grade Zn(II) carbonate basic (Alfa Aesar, U.K., 99 wt.%), hydrate Ce(III) carbonate (Treibacher Industrie AG., Germany, 99 wt.%), and reagent grade aqueous methanesulfonic acid (Sigma Aldrich, U.K., 70 vol.%) were used as received. All solutions were prepared with ultra-pure water (18 MΩ cm resistivity) from an Elga water purification system. Zinc(II) and cerium(III) methanesulfonates of 2 mol $dm^{-3}$ were prepared by stirring 0.4 mol $dm^{-3}$ zinc carbonate basic and 1 mol $dm^{-3}$ cerium carbonate powders in 10 and 6 mol $dm^{-3}$ aqueous methanesulfonic acid, respectively, using a PTFE-coated steel magnetic stirred bar (Fisherband, U.K., 1 cm diameter, 4 cm length). During the preparation of Ce(III) methanesulfonate, the temperature was maintained at 80 °C for 6 h using a hot-plate stirrer (Ika Yellowline®) [24,33,34]. The resulting Zn(II) and Ce(III) methanesulfonate solutions were colourless with no precipitate.

### 2.2. Cyclic voltammetry

A typical divided, three-electrode glass cell with approximately 160 $cm^3$ of electrolyte volume in the working electrode compartment separated from the counter electrode by a Nafion® membrane (Dupont, NF117/$H^+$, USA) was used. This glass cell was equipped with a water jacket connected to a water thermostat controller (Grant, Model LV FG., UK) to maintain the temperature in the range of 20–60 °C. For the half-cell reactions of Zn and Ce, the working electrodes (area: 0.13 $cm^2$) were glassy carbon and platinum disc, respectively. The counter electrode was a platinum mesh (area: 1 $cm^2$). The electrode potentials were measured against a saturated Ag|AgCl electrode (ABB, Series 1400, 0.1 mol $dm^{-3}$ $KNO_3$). The electrochemical measurements were made using an EcoChemie Autolab (PGSTAT20, Netherlands) computer controlled potentiostat and General Purpose, Electrochemical Software (GPES) Version 4.5.

### 2.3. Flow battery experiment

The electrical and electrolytic circuits of the flow battery are shown in Fig. 1a. An expanded view of the flow cell (102 mm × 47 mm × 45 mm dimensions) is shown in Fig. 1b. The cell was manufactured with a polyvinyl chloride (PVC) casing, two acrylic (Perspex®) flow channels, four 1.5 mm thickness rubber silicon gaskets as well as the negative and positive electrodes, separated by a cation-conducting Nafion® membrane (DuPont, NF117/$H^+$, USA). The dimensions of each electrode were 70 mm × 50 mm and were fitted with a silicone rubber gasket to expose an active surface area of 9 $cm^2$ (45 mm × 20 mm) to the electrolyte. The membrane-electrode gap was 11 mm. The electrolytes (100 $cm^3$ each) were contained in separate tanks.

Carbon polyvinyl-ester composite (Engtegris Inc., BMC 18649, Germany) was used as the negative electrode and a range of positive electrode materials were tested. A detailed description of the positive electrode materials used in this work is given in Table 1. The platinised titanium mesh was manufactured by spot welding four pieces of platinised titanium mesh (44 mm × 16 mm × 2.5 mm each, 70 g Pt $m^{-2}$ loading, Magneto GmbH, Netherlands) onto a planar platinised titanium plate (70 g Pt $m^{-2}$ loading, Magneto GmbH, Netherlands). Other three-dimensional positive electrode materials such as reticulated vitreous carbon and carbon felt were heat-bonded to a graphite plate using a conductive carbon adhesive (Binder & Cotronics Corp., 931, USA). After compressing the electrode to the graphite plate overnight, the adhesive was cured at 130 °C for 4 h.

Unless otherwise stated, the positive electrolyte contained 0.8 mol $dm^{-3}$ Ce(III) methanesulfonate in 4.0 mol $dm^{-3}$ methanesulfonic acid, while the negative electrolyte compartment contained 1.5 mol $dm^{-3}$ Zn(II) methanesulfonate in 1.0 mol $dm^{-3}$ methanesulfonic acid. The electrolytes were maintained at 50 °C by a water thermostat (Grant, Model LV FG, UK) through water jackets fitted to the containers. Both positive and negative electrolytes were circulated through the cell at 3.9 cm $s^{-1}$ using two peristaltic pumps (Cole-Parmer, Masterflex® Model 7553079) with high-pressure tubings (Masterflex® Norprene®, Cole-Parmer, 6 mm inner diameter). Saturated Ag|AgCl electrodes served as reference electrodes (ABB, Series 1400, 0.1 mol $dm^{-3}$ $KNO_3$) placed in line at the entrance of each flow channel.

In a typical experiment, the battery was charged at 450 mA (50 mA $cm^{-2}$ with respect to the two-dimensional electrode) for 4 h. The current density reported in this paper is always referred to the negative 2D electrode but due to the higher surface areas of the positive electrodes tested, the current density on these electrodes would be smaller. After charge, the cell was left at open-circuit potential for 1 min and discharged at the same current. Cut-off voltages were set at 3.4 V and 0.5 V during battery charge and discharge, respectively. All electrochemical measurements were made using a BaSyTec (5A/12V, Germany) battery test system. The anode, cathode and cell potentials were continuously monitored.

### 2.4. Determination of the Ce(IV) concentration

A 0.5 $cm^3$ aliquot of positive electrolyte solution was removed during the charge and discharge cycles at regular intervals of time. The concentration of Ce(IV) in methanesulfonic acid contained in this aliquot was determined by a titration method as outlined in previous studies [35–37]. The 0.5 $cm^3$ volume of unknown concentration of Ce(IV) was mixed with 9.5 $cm^3$ of 2.0 mol $dm^{-3}$ methanesulfonic acid and ferroin (1,10 orthophenanthroline–ferrous sulphate complex, Fluka) as a colorimetric redox indicator. A freshly prepared solution of 0.01 mol $dm^{-3}$ $NH_4Fe(II)$ was used to titrate the solution of unknown Ce(IV) ion concentration. The concentration of Ce(IV) was then determined from the

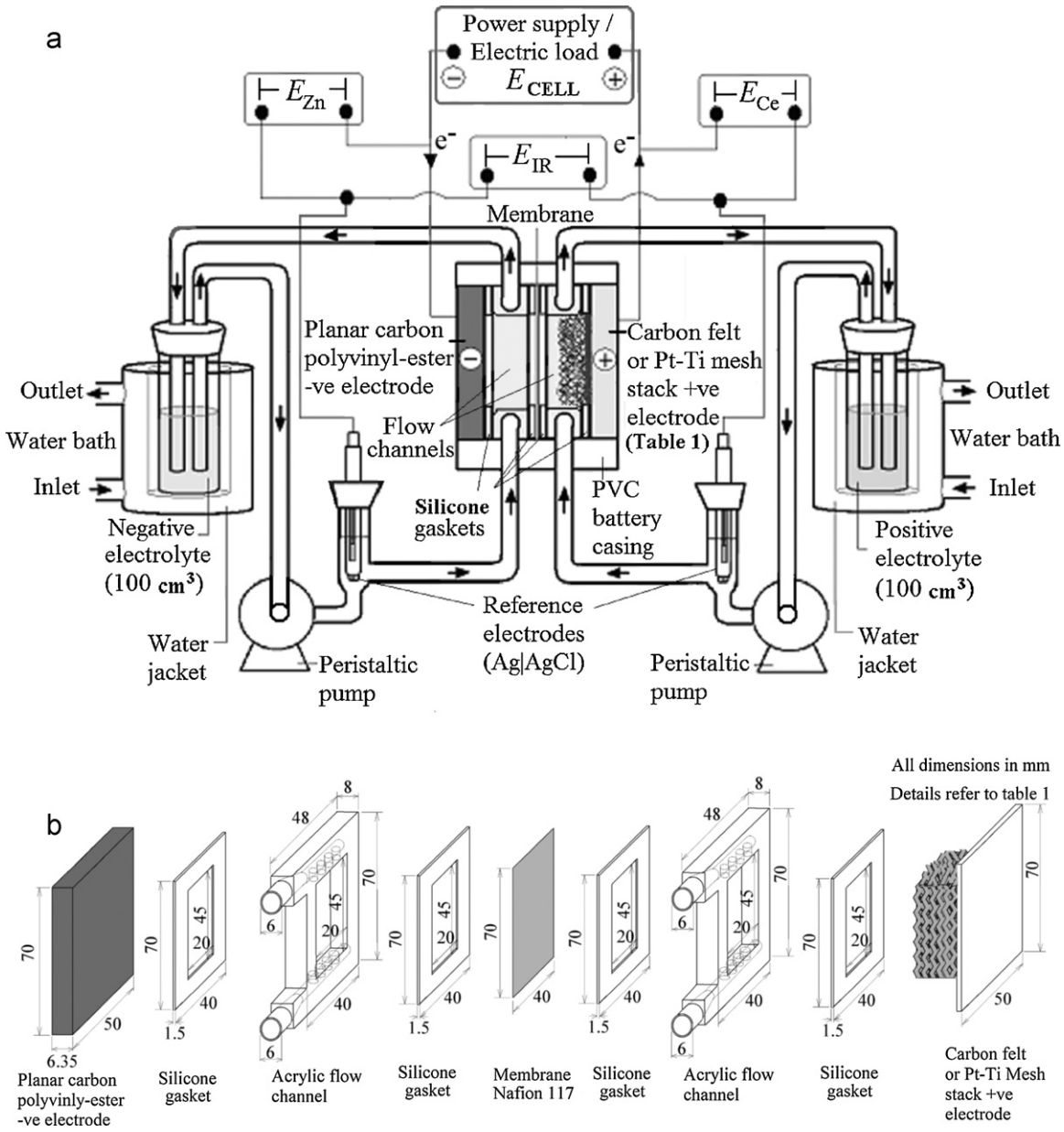


**Fig. 1.** Experimental arrangement and electrical circuit of a zinc cerium redox flow battery. (a) Overall set-up showing the points of measurement of the cell potential $E_{cell}$, the potential of the positive and negative electrodes, $E_{Ce}$ and $E_{Zn}$, respectively and the ohmic voltage drop across the membrane $E_{IR}$ and (b) expanded view of the components of a flow battery. The units are shown in mm.

amount of Fe(II) required to achieve complete reduction of Ce(IV) to Ce(III).

## 3. Results and discussions

### 3.1. Electrochemistry of zinc and cerium in methanesulfonic acid

Fig. 2 shows the combined cyclic voltammogram of the Zn and Ce half-cell reactions under static conditions at different temperatures. The voltammogram of Zn was carried out between −0.7 and −1.2 V *vs.* Ag|AgCl at 128 mV $s^{-1}$ in the negative electrolyte containing 1.5 mol $dm^{-3}$ Zn(II) methanesulfonate and 1 mol $dm^{-3}$ methanesulfonic acid on a glassy carbon disc electrode (0.13 $cm^2$). The behaviour of the Ce half-cell reaction was recorded between +0.5 and +1.9 *vs.* Ag|AgCl at 128 mV $s^{-1}$ in the positive electrolyte containing 0.8 mol $dm^{-3}$ Ce(III) methanesulfonate and 4 mol $dm^{-3}$ methanesulfonic acid using a platinum electrode (0.13 $cm^2$).

The cyclic voltammograms show that temperature has a much greater influence on the peak currents of the Zn reaction compared to those associated with the Ce reaction. The current density of Zn reduction increased tenfold when the temperature changed from 22 to 60 °C, whereas the oxidation current of Ce(III) was only doubled. It is also likely that hydrogen evolution (reaction (2)) contributed to the current for Zn electrodepositon, while oxygen evolution (reaction (4)) may have affected the current for Ce(III) oxidation. During charge, Zn(II) electrodeposition and Ce(III) oxidation take place at *c.a.*−1.08 V and +1.84 V *vs.* Ag|AgCl, respectively at 22 °C. During discharge, dissolution of Zn(0) occurs at −0.94 V *vs.* Ag|AgCl together with the reduction of Ce(IV) at +1.05 V *vs.* Ag|AgCl. A simple estimation of the charge and discharge cell voltages can be obtained by subtracting the Zn potential from the Ce potential. At 22 °C, the estimated values for charge and discharge would be 2.92 V and 1.99 V, respectively. An estimation of the charge and discharge cell voltages at 60 °C yields 2.81 V and 2.08 V, respectively.

**Table 1**
Positive electrode materials evaluated for the zinc–cerium redox flow battery.

| Type | Electrode materials | Details | Specific surface area ($cm^2\ cm^{-3}$) | Total surface area ($cm^2$) | Observations | | Ce(IV) after 4 h charge at 50 mA $cm^{-2}$ ($mol^{-1}\ dm^{-3}$) |
|---|---|---|---|---|---|---|---|
| | | | | | Electrode | Electrolyte | |
| 1 | Platinised titanium (7 cm × 5 cm × 0.2 cm) | 70 g Pt $m^{-2}$ loading, 3. 5 μm thick, Magneto GmbH (Netherlands) | Nil (2D) | 9 | Stable, no observable change | Clear yellowish solution | 0.456 |
| 2 | Graphite (7 cm × 5 cm × 0.6 cm) | Grade S plate, Le Carbone Lorraine S.A. (France) | Nil (2D) | 9 | Graphite plate exfoliated, as particles came off after 10 min | Very dark solution with carbon particles | 0.104 |
| 3 | Carbon–polyvinylester (7 cm × 5 cm × 0.6 cm) | BMC 18649 Vinyl ester bipolar plate Entegris Inc. (Germany) | Nil (2D) | 9 | Carbon plate exfoliated, as particles came off after 10 min | Very dark solution with carbon particles | 0.08 |
| 4 | 30 ppi reticulated vitreous carbon (4.5 cm × 2 cm × 2 cm) | Duocel®, ERG Material and Aerospace Corp. (USA) | 19 [46] | 342 | Slightly expanded, and carbon particles came off after 2 h and 15 min | Dark solution with carbon particles | 0.16 |
| 5 | 100 ppi reticulated vitreous carbon (4.5 cm × 2 cm × 2 cm) | Duocel®, ERG Material and Aerospace Corp. (USA) | 65 [46] | 1170 | Slightly expanded, and carbon particles came off after 2 h and 15 min | Dark solution with carbon particles | 0.128 |
| 6 | Alfa Aesar carbon felt (4.5 cm × 2 cm × 0.8 cm) | Stock 42107, 99%, Alfa Aesar (UK) | 452.3 [47] | 3256 | Became darker the appearance after the experiment | Clear orange solution with very few carbon particles | 0.632 |
| 7 | Sigratherm® carbon felt (4.5 cm × 2 cm × 0.8 cm) | GFA -05, SGL Group (Germany) | 240–600 [48] | 1728–4320 | No observable change in appearance | Clear orange solution with very few carbon particles | 0.656 |
| 8 | 4 Platinised titanium mesh (4.4 cm × 1.6 cm × 0.25 cm each) welded on a platinised titanium plate (7 cm ×5 cm × 0.2 cm) | 70 g Pt $m^{-2}$ loading, 3.5 μm thick, Magneto GmbH(Netherlands) | 19.3 | 72.7 | Stable, no observable change | Clear orange solution | 0.652 |

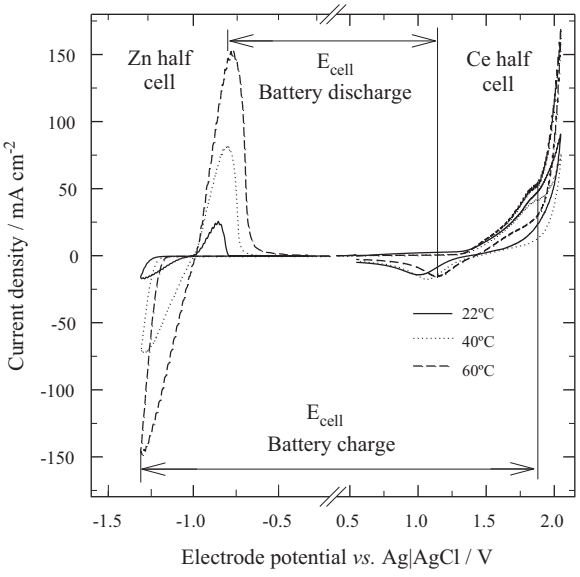


**Fig. 2.** A combined cyclic voltammetry of zinc half-cell at glassy carbon electrode and cerium half-cell reaction at platinum sweeping the potential linearly at 128 mV $s^{-1}$ from +0.5 to +1.9 V *vs.* Ag|AgCl and −0.7 to −1.2 V *vs.* Ag|AgCl, respectively at electrolyte temperatures of 20, 40 and 60 °C. Negative electrolyte: 1.5 mol $dm^{-3}$ zinc(II) methanesulfonate and 1 mol $dm^{-3}$ methanesulfonic acid. Positive electrolyte: 0.8 mol $dm^{-3}$ cerium(III) methanesulfonate and 4 mol $dm^{-3}$ methanesulfonic acid.

These values do not include the ohmic losses across the electrolyte, electrodes and membrane. They do demonstrate, nevertheless, the increased voltage efficiency with higher temperature.

As the temperature was increased, the separation between the oxidation and reduction peaks of each redox couple decreased. For the Zn(0)/Zn(II) redox couple, the separation decreased by 30 mV and for the Ce(III)/Ce(IV) redox couple the separation decreased by 150 mV. At increased temperatures, the oxidation and reduction peak current density of both zinc and cerium reactions also increased. The cyclic voltammetry shows that the positive electrode reaction could limit the use of high currents. High surface area electrodes could be used to solve this problem. A range of two- and three-dimensional positive electrodes were, therefore, investigated, as detailed in the next section.

### 3.2. Selection of the positive electrode materials

A summary of the characteristics and behaviour of the eight positive electrode materials tested in a Zn/Ce redox flow battery (at 50 °C) is shown in Table 1. A carbon polyvinyl-ester composite was used as the negative electrode material. Both the positive and negative electrolyte compositions were the same as those used for the cyclic voltammetry described in Section 3.1 and were circulated through the respective half-cells with a mean linear flow velocity of 3.9 cm $s^{-1}$. The battery was first charged at 50 mA $cm^{-2}$ for 4 h using different electrodes, after which the concentration of Ce(IV) was measured. These concentrations are shown in Table 1. The battery was then discharged at different

constant current densities in the range 5–50 mA cm$^{-2}$ and different constant cell voltages in the range 2.2–1.0 V. In order to keep the Ce(IV) concentration approximately constant, each discharge current or voltage was applied for only 2 min, enough time to measure the cell voltage or current generated. The battery was recharged frequently to restore the concentration of Ce(IV) ions and maintain the same state of charge (SOC) for each experiment.

Table 1 shows that during charge at 50 mA cm$^{-2}$, the conversion of Ce(III) was highest when the two carbon felts and the three-dimensional platinised titanium mesh were used. Ce(IV) concentrations reached more than 0.60 mol dm$^{-3}$ at current efficiencies of >90% using these electrodes. Platinum-based positive electrode materials were stable throughout the battery charge and discharge cycles [38]. The reticulated vitreous carbon, graphite and carbon polyvinyl-ester composite exhibited less stability and poorer performance as well as lower Ce(IV) conversion. These electrodes either exfoliated or expanded and carbon sludge appeared in the electrolytes during charge-discharge cycles. These observations and the changes in the electrolyte conditions are summarized for the eight positive electrodes tested in Table 1.

### 3.2.1. Constant current density and constant voltage discharge

The patented zinc–cerium system discharges at a constant cell voltage of 1.8 V [19,20], at which the current density undergoes an exponential decay. Despite a high initial current density, the full discharge of the battery requires a prolonged period of time [15]. In practice, constant current density discharge is preferred due to lower cost and a more steady power output. Fig. 3a shows the initial cell voltages of the eight positive electrode materials *vs.* a constant discharge current density (5–50 mA cm$^{-2}$). With all materials, the cell voltage decreased as the applied current density increased. This is attributed to the electrode overpotentials and ohmic drop across the electrodes, electrolytes and membrane. The majority of the two-dimensional materials and the reticulated vitreous carbon electrodes exhibited a large cell voltage drop during discharge at increased current densities.

The initial cell voltages using the carbon felts and the three-dimensional platinised titanium mesh were all above 1.8 V at current densities in the range 5–50 mA cm$^{-2}$, with less than a 0.55 V drop in the voltage. The high cell voltages were due to the high Ce(IV) concentration generated in the positive electrolyte (Table 1) and to the low local current density of the large surface area of the electrodes. In contrast, the two-dimensional platinised titanium electrode, the carbon polyvinylester and the reticulated vitreous carbon exhibited voltage drops of more than 1.5 V when the discharge current density increased from 20 to 25 mA cm$^{-2}$. This was possibly due to a low concentration of Ce(IV) near the electrode surface, which lead to an appreciable rate of hydrogen evolution. It is important to note that despite its high surface area, the performance of reticulated vitreous carbon electrodes is similar to that of the two-dimensional electrodes.

A similar picture emerged with a constant cell voltage discharge (1.0–2.2 V) after the 4 h charge at 50 mA cm$^{-2}$ (Fig. 3b). The highest initial current densities were obtained with the two carbon felts and the platinised titanium mesh electrodes. The current densities associated with the two-dimensional electrodes and the reticulated vitreous carbon materials were appreciably lower. In the cases of the two carbon felts and the platinised titanium mesh electrode, the large current densities obtained at low discharge cell voltages were again due to hydrogen evolution. Discharging the zinc–cerium battery at such low voltages is not a practical approach (high rates of hydrogen evolution and lower efficiencies).

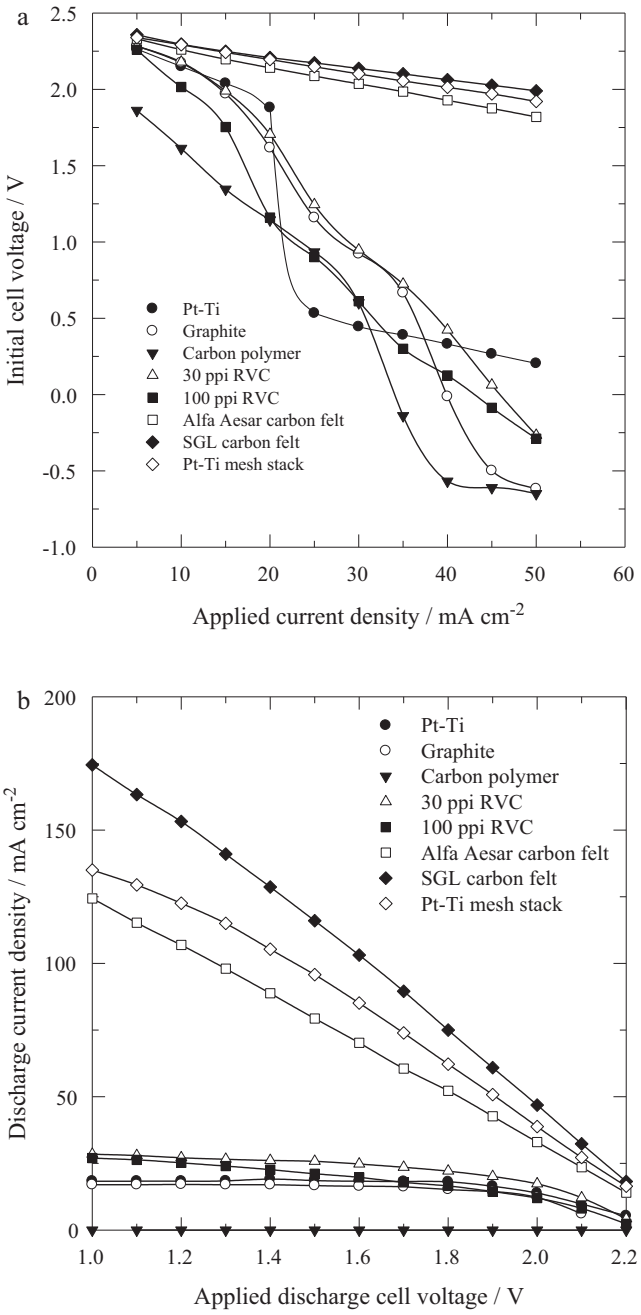


**Fig. 3.** Performance of 8 positive electrode materials in a zinc–cerium redox flow battery during the discharge cycle. (a) Constant current density. (b) Constant cell voltage; carbon–polyvinylester composite was used as a negative electrode material. Negative electrolyte was 100 cm$^3$ solution containing 1.5 mol dm$^{-3}$ zinc(II) methanesulfonate in 1 mol dm$^{-3}$ methanesulfonic acid. Positive electrolyte was 100 cm$^3$ solution containing 0.8 mol dm$^{-3}$ cerium (III) methanesulfonate in 4 mol dm$^{-3}$ methanesulfonic acid. Both negative and positive electrolytes were circulated at 3.9 cm s$^{-1}$ by a peristaltic pump and maintained at 50 °C by a water bath. (●) 2-d Pt-Ti, (○) graphite, (▼) carbon polyvinyl-ester, (△) 30 ppi reticulated vitreous carbon, (■) 100 ppi reticulated vitreous carbon, (□) Alfa-Aesar carbon felt, (♦) SGL carbon felt and (◊) Pt–Ti mesh stack.

### 3.3. Charge/discharge performance of a zinc–cerium redox flow battery

Based on the above results, it was concluded that carbon felt and platinised titanium mesh are the optimum positive electrode materials. The charge–discharge performance of the redox flow battery was studied using Sigratherm® GFA-05 carbon felt and the pla-

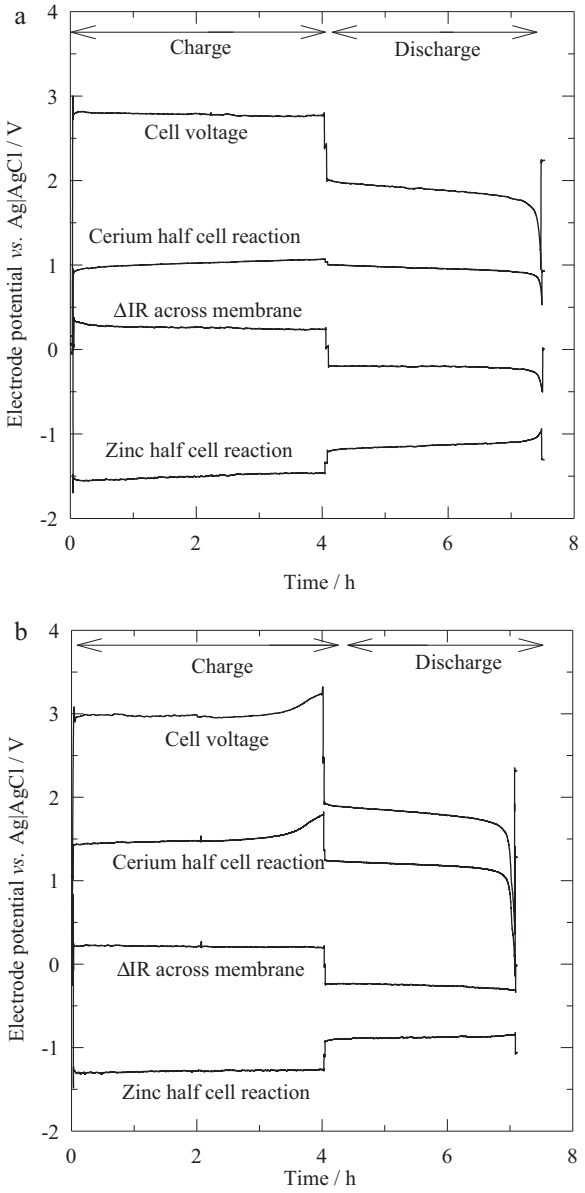


**Fig. 4.** Voltage *vs.* time characteristics of a zinc–cerium redox flow battery equipped with high surface areas of positive electrodes: (a) Sigratherm® carbon felt and (b) platinised titanium mesh electrodes. Electrolyte composition and operating conditions as in Fig. 3.

tinised titanium mesh as the positive electrodes, while the negative electrode consisted of a carbon polyvinyl-ester composite.

The cell voltage and electrode potentials using the GFA-05 felt and the platinised titanium mesh are shown in Fig. 4a and b, respectively. These figures also show the ohmic drops across the membrane and electrolyte during the 4 h charge/discharge cycle. The charge/discharge performance with the Sigratherm® carbon felt was superior. Using the platinised titanium mesh, the cell voltage began to rise after 3 h of charging, due to significant Ce(III) consumption and oxygen evolution in the positive electrode. With the Sigratherm® carbon felt, the coulombic efficiency was 92.4% and the energy efficiency at 50 mA cm$^{-2}$ was 63%, which compares well with other systems such as the soluble lead acid flow battery (around 58% at 40–60 mA cm$^{-2}$ [40]). The platinised titanium mesh yielded a coulombic efficiency of 71% and an energy efficiency of 43% at 50 mA cm$^{-2}$.

In the zinc–cerium battery fitted with a Sigratherm® carbon felt positive electrode, the change in the cerium half-cell potential between the charge and discharge cycle was only 0.07 V, compared to 0.29 V using the platinised titanium mesh electrode (Fig. 4a and b). This value of 0.29 V is smaller than the equivalent half-cell voltages in the zinc–chlorine [41] and zinc–bromine [39] systems. In addition to this advantage, carbon felt is less expensive than platinum and does not form an oxide layer during the oxidation of Ce(III) [42], i.e., the Ce redox reaction at the carbon felt electrode exhibits a greater degree of reversibility.

The carbon polyvinyl-ester composite negative electrode material in both systems (Fig. 4a and b) yielded a half-cell potential difference of 0.35 V between charge and discharge cycles. This value is larger than the equivalent values for the zinc–chloride [41] and zinc–bromide [39] systems, possibly due to the high stability of the Zn(II) methanesulfonate complexes. Additives, such as indium oxide [21], can be used to reduce the overpotentials in aqueous methanesulfonic acid. The reduction of Ce(IV) took slightly longer in the battery using the Sigratherm® carbon felt (see Fig. 4a and b). Fig. 4b also shows that zinc deposits remained on the mesh electrode at the end of the discharge cycles. In contrast, zinc electrodeposits were stripped away after discharging for 3.4 h, as indicated by the potential increase towards the end of the cycle in Fig. 4a. Both the zinc and cerium electrodes were completely utilized during battery discharge using the carbon felt. In the cell based on the platinised-titanium mesh electrode, the Ce half-cell reaction was the main limiting factor in the system. Despite the high efficiency of carbon felts as positive electrodes, poor conductivity and poor adherence of the carbon adhesive were observed after 2–3 charge/discharge cycles. Further developments on the construction of such electrodes and the connections in the highly acidic, oxidizing Ce(IV) methanesulfonate electrolyte are required.

### 3.4. Effect of flow conditions on battery discharge

In RFBs, mass-transport conditions play an important role in delivering a large power output. The effect of the mean linear flow velocity of the electrolyte on the battery performance was studied under constant current density and constant voltage discharge. The Sigratherm® carbon felt and platinised titanium mesh were again used as the positive electrodes, while the negative electrode was a carbon–polyvinylester composite. The battery was first charged at current density of 50 mA cm$^{-2}$ (referred to the negative electrode area) for 4 h in order to achieve the same state of charge (SOC) before all tests. The battery was then discharged at a range of constant current densities (10–70 mA cm$^{-2}$) and cell voltages (1.0–2.2 V) under a wide range of mean linear electrolyte flow velocities (1.2–7.8 cm s$^{-1}$). In order to maintain the Ce(IV) concentration constant, each current and potential was applied for 2 min only and the battery was frequently charged between measurements to restore the Ce(IV) consumed and maintain the same state of charge SOC.

The effect of the flow velocity on the discharge current densities at constant cell voltage discharge, for both positive-electrode materials, is shown in Fig. 5. At a fixed cell voltage, the current density increased with increased flow velocity; the changes were more pronounced when the Sigratherm® carbon felt was used (Fig. 5a), for which the discharge current densities reached their maximum values at 3.9 cm s$^{-1}$ for all cell voltages. In the cell using a platinised titanium mesh, the optimum flow velocity was also 3.9 cm s$^{-1}$, though the peak is less pronounced (Fig. 5b). As the velocity is increased, polarization losses would be expected to be lower at equivalent states of charge since the reactants would be distributed more evenly and the width of any Nernst diffusion layer decreased.

Fig. 5c and d show the effect of the mean linear flow velocity on the discharge voltage at a constant discharge current density. The maximum cell voltages using the Sigratherm® carbon felt were again found to occur at a velocity of 3.9 cm s$^{-1}$. In contrast, the

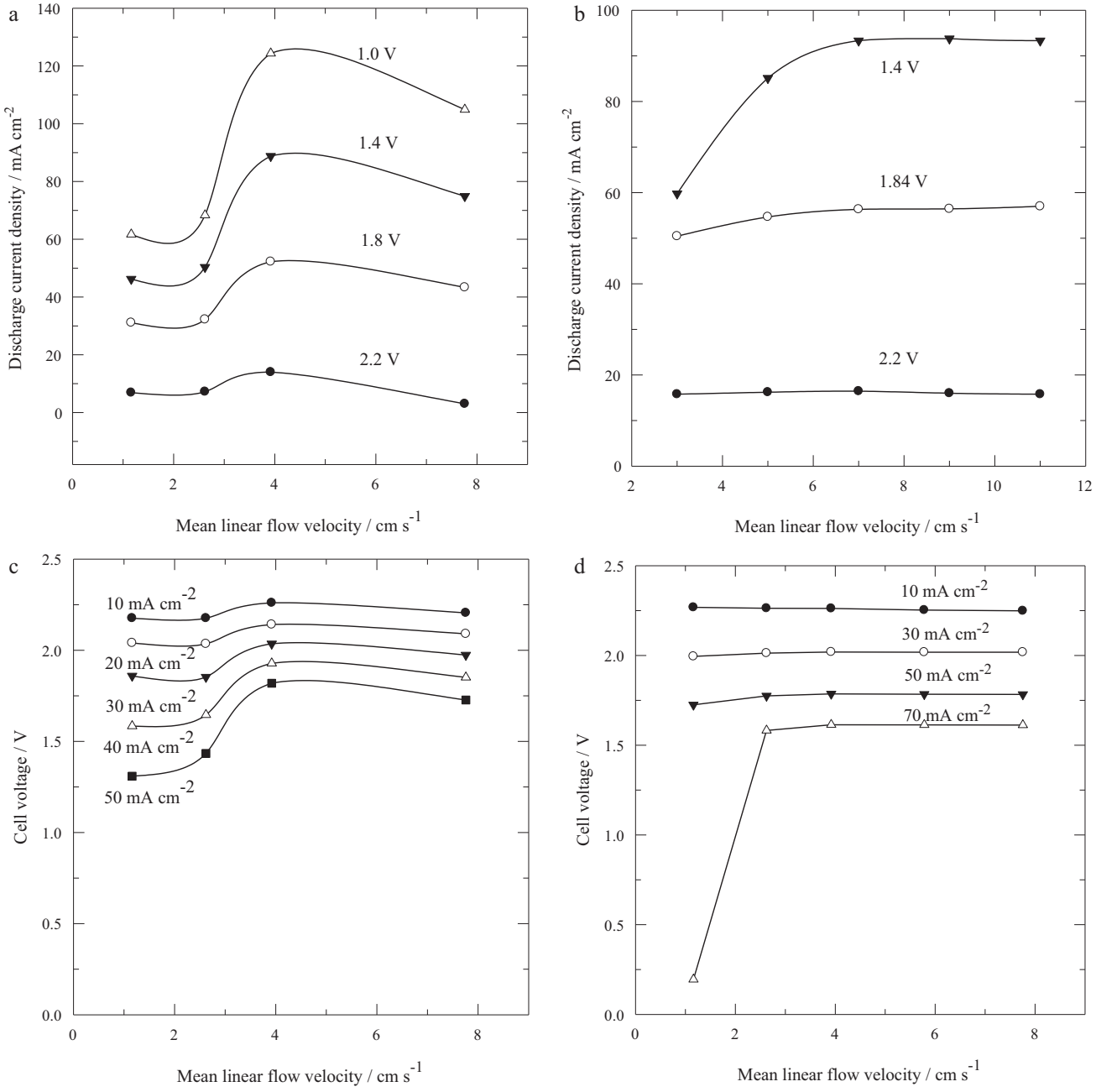


**Fig. 5.** Effect of flow condition on discharge performance of a zinc–cerium redox flow battery. (a) Constant voltage discharge at Sigratherm® carbon felt, (b) constant voltage discharge at platinised titanium mesh electrode, (c) constant current density discharge at Sigratherm® carbon felt and (d) constant current density discharge at platinised titanium mesh electrode. Electrolyte compositions and operating conditions were the same as in Fig. 3.

cell voltages obtained using the platinised titanium mesh remained almost constant over a wide range of flow velocities, except for a discharge current density of 70 mA $cm^{-2}$. At this value, high flow velocities (>2.62 cm $s^{-1}$) are required to offset the rapid Ce(IV) depletion.

### 3.5. Efficiencies of a zinc–cerium flow battery

In order to determine the optimum operating conditions and electrolyte compositions of a zinc–cerium flow battery, experiments were carried out over a broad range of operating conditions and electrolyte compositions. A platinised titanium mesh was used as the positive electrode. The flow battery was first charged for 4 h at a constant current and discharged at the same current until the cell voltage dropped below 0.5 V. Table 2 summarizes the charge–discharge voltages and the system efficiencies when the parameters were changed (discussed below). In all cases, the Ce half-cell was the limiting reaction for battery discharge since the redox reaction of Zn continued for longer than the cerium reaction, during both charge and discharge.

#### 3.5.1. Operating parameters

Fig. 6a shows the charge–discharge performance at constant current density. A smaller cell voltage drop between the charge and discharge cycles was observed at low current densities, hence the voltage efficiency improved. At a higher current density, Ce(III) depletes more rapidly during charge at the positive electrode, leading to a higher potential and, therefore, an increased rate

**Table 2**
System efficiencies of a zinc–cerium redox flow battery at different operating compositions and electrolyte compositions. Unless specified, the operating conditions are the same as in Fig. 3.

| Operating parameters | Average charge voltage (V) | Average discharge voltage (V) | [Ce(IV)] after charge (mol dm$^{-3}$) | [Ce(IV)] after discharge (mol dm$^{-3}$) | % Coulombic efficiency | % Voltage efficiency | % Energy efficiency |
|---|---|---|---|---|---|---|---|
| Current density (mA cm$^{-2}$) | | | | | | | |
| 20 | 2.67 | 1.98 | 0.264 | 0.098 | 63.1 | 74.2 | 46.8 |
| 50 | 2.98 | 1.79 | 0.652 | 0.184 | 71.4 | 60.1 | 42.9 |
| 80 | 3.33 | 1.57 | 0.728 | 0.271 | 43.6 | 47.1 | 20.5 |
| Temperature (°C) | | | | | | | |
| 25 | 3.30 | 1.55 | 0.600 | 0.288 | 47.6 | 47.0 | 22.4 |
| 40 | 3.13 | 1.61 | 0.616 | 0.218 | 60.7 | 51.4 | 31.2 |
| 50 | 2.98 | 1.79 | 0.652 | 0.184 | 71.4 | 60.1 | 42.9 |
| 60 | 2.86 | 1.82 | 0.672 | 0.260 | 62.8 | 63.6 | 39.9 |
| Mean linear electrolyte flow velocity (cm s$^{-1}$) | | | | | | | |
| 1.16 | 3.15 | 1.61 | 0.640 | 0.396 | 37.3 | 51.1 | 19.1 |
| 1.79 | 3.02 | 1.74 | 0.616 | 0.280 | 51.4 | 57.6 | 29.6 |
| 3.92 | 2.98 | 1.79 | 0.652 | 0.184 | 71.4 | 60.1 | 42.9 |
| 5.78 | 2.93 | 1.74 | 0.669 | 0.201 | 71.4 | 59.4 | 42.4 |
| [Ce(III)] (mol dm$^{-3}$) | | | | | | | |
| 0.4 (2.5 h electrolysis) | 3.08 | 1.73 | 0.385 | 0166 | 56.0 | 56.2 | 31.5 |
| 0.8 | 2.98 | 1.79 | 0.652 | 0.184 | 71.4 | 60.1 | 42.9 |
| 1.0 | 3.01 | 1.72 | 0.632 | 0.237 | 60.3 | 57.1 | 34.5 |
| 1.2 | 3.04 | 1.65 | 0.628 | 0.293 | 51.1 | 54.3 | 27.7 |
| [Zn(II)] (mol dm$^{-3}$) | | | | | | | |
| 0.5 | 2.99 | 1.80 | 0.652 | 0.204 | 68.4 | 60.2 | 41.2 |
| 1 | 2.98 | 1.77 | 0.652 | 0.179 | 72.2 | 59.4 | 42.9 |
| 1.5 | 2.98 | 1.79 | 0.652 | 0.184 | 71.4 | 60.1 | 42.9 |
| 2 | 3.13 | 1.51 | 0.652 | 0.201 | 69.0 | 48.2 | 33.3 |
| [Methanesulfonic acid] in positive electrolyte (mol dm$^{-3}$) | | | | | | | |
| 2 | 3.01 | No discharge (insoluble) | 0.616 | No discharge | Nil | Nil | Nil |
| 3 | 3.01 | 1.74 | 0.608 | 0.307 | 45.9 | 57.8 | 26.6 |
| 4 | 2.98 | 1.79 | 0.652 | 0.185 | 71.4 | 60.1 | 42.9 |
| 5 | 3.00 | 1.68 | 0.656 | 0.291 | 55.7 | 56.0 | 31.2 |

of oxygen evolution. The low coulombic efficiencies observed at 20 and 80 mA cm$^{-2}$ (Table 2) were due to a combination of limited mass transport of Ce(IV) ions and the secondary reactions. For instance, the Ce(IV) concentrations after discharge at 20 and 80 mA cm$^{-2}$ were 0.098 and 0.271 mol dm$^{-3}$, respectively.

Fig. 6b shows the effect of flow velocity on the charge–discharge cycle. Higher coulombic and voltage efficiencies were obtained as the flow velocity increased up to 3.9 cm s$^{-1}$, indicating again the importance of reactant mass transport during discharge. Additionally, the improved supply of zinc and cerium ions towards the electrodes reduces the effects of side reactions. Further increases in mean linear electrolyte flow velocity above 3.9 cm s$^{-1}$ did not yield any improvements since the reaction was no longer mass-transport controlled.

The effects of temperature on the charge–discharge performance are shown in Fig. 6c. Substantial improvements in both the charge and voltage efficiencies were obtained as the temperature increased from 25 to 50 °C. The coulombic efficiency increase was due to faster reaction kinetics, increased diffusion rates and a reduced viscosity. Higher voltage efficiencies were attributed to the increased electrolyte conductivity (decreased overpotentials) [32,43].

### 3.5.2. Electrolyte composition

The electrolyte compositions have a large influence on the charge/discharge performance of a zinc–cerium battery. The previous section demonstrated that the Ce half-cell reaction was the limiting factor at all operating conditions. Optimize the composition of the positive electrolyte is, therefore, crucial to the development of the system. Fig. 7a and b shows the cell voltage characteristics of the cell for different concentrations of Ce(III) and methanesulfonic acid in the positive electrolyte, respectively. In both figures, the cell voltage increases after 2 h of charging, with oxygen evolution becoming the main reaction when the concentration of Ce(III) ions gradually falls. The data in Table 2 shows that for Ce(III) ion concentrations higher than 0.8 mol dm$^{-3}$, the concentration of Ce(IV) generated at the end of the charge cycle drops, which is consistent with previous results using platinum as the positive electrode [43]. Increasing the Ce(III) concentration from 0.8 to 1.2 mol dm$^{-3}$ decreased the voltage and coulombic efficiencies (Table 2) since the solutions became viscous and milky. This was mainly due to the low Ce(III) solubility in 4 mol dm$^{-3}$ methanesulfonic acid. It has been reported that a high concentration of Ce(III) can only be obtained at low methanesulfonic acid concentrations [25]. In contrast, higher Ce(IV) concentrations are only soluble in concentrated methanesulfonic acid [25]. The solubility limit of both Ce(III) and Ce(IV) in 4.0 mol dm$^{-3}$ methanesulfonic acid is *c.a.* 1.0 mol dm$^{-3}$ at room temperature [25,44].

Increasing the methanesulfonic acid concentration up to 4 mol dm$^{-3}$ in the positive electrolyte can increase both the voltage and coulombic efficiencies (Fig. 7b). For methanesulfonic acid concentrations of 2 and 3 mol dm$^{-3}$, the positive electrolyte was highly viscous after battery charge. This suggests that highly concentrated Ce(IV) solutions will be difficult to achieve in methanesulfonic acid concentrations lower than 4 mol dm$^{-3}$. The discharge behaviour using such electrolytes was unfavorable, resulting in poor coulombic efficiencies. No battery discharge was observed for the 2 mol dm$^{-3}$ methanesulfonic acid solution. Taking into account the battery performance and the solubility of Ce(IV) ions in low concentrations of acid, the optimum positive electrolyte composition was determined to be 0.8 mol dm$^{-3}$ Ce(III) methanesulfonate in 4 mol dm$^{-3}$ methanesulfonic acid.

The solubility problem of Zn(II) methanesulfonate is less complicated. As summarized in Table 2, higher cell voltages during charge

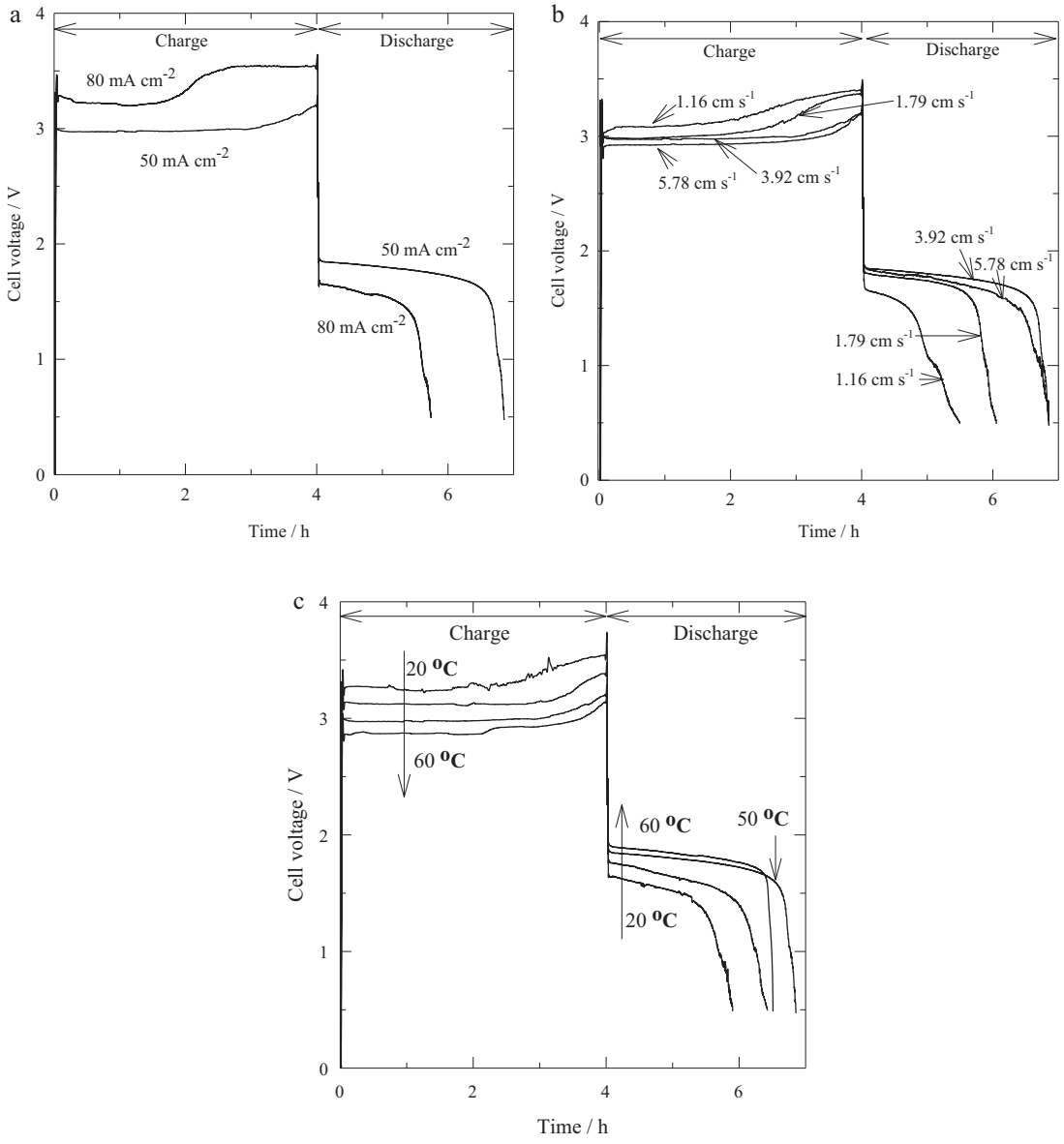


**Fig. 6.** Effect of operating conditions on the charge–discharge performance of a zinc–cerium redox flow battery: (a) current density, (b) mean linear electrolyte flow velocity and (c) temperature. Unless indicated, electrolyte compositions and operating conditions were the same as in Fig. 3.

and lower discharge cell voltages were observed at 2 mol dm$^{-3}$ Zn(II), close to the solubility limit (2.16 mol dm$^{-3}$) in methanesulfonic acid [24]. For a Zn(II) methanesulfonate concentration in the range 0.5–1.5 mol dm$^{-3}$, no significant effect on either the coulombic or the voltage efficiency was observed. Higher Zn(II) ion concentrations, e.g. 1.5 mol dm$^{-3}$, can, on the other hand, be advantageous at high current densities in order to avoid mass transport limitation.

### 3.6. Life cycle

A number of charge–discharge experiments at the optimum operating conditions and electrolyte compositions (0.8 mol dm$^{-3}$ Ce(III) methanesulfonate in 4.0 mol dm$^{-3}$ methanesulfonic acid, 1.5 mol dm$^{-3}$ Zn(II) methanesulfonate in 1.0 mol dm$^{-3}$ methanesulfonic acid) were carried out on the zinc–cerium flow battery to investigate life cycle effects. The charge–discharge characteristics at different states of charge were recorded by charging at 50 mA cm$^{-2}$ for different lengths of time: 15 min (Fig. 8a), 1 h, 2 h, and 4 h (Fig. 8b). In a further experiment, the battery was first charged at 50 mA cm$^{-2}$ for 3 h following 15 min charge/discharge cycles for approximately 14 h (see Fig. 9). During charge and discharge, cut-off cell voltages were set at 3.4 V and 0.5 V, respectively. A platinised titanium mesh was used as the positive electrode, while the negative electrode was a carbon–polyvinylester composite.

The life cycle and system efficiencies of these experiments are summarized in Table 3. As shown in Fig. 8a and b, the maximum number of cycles that the battery was able to perform (before no discharge could be obtained) increased from 4 cycles in the 4 h charge/discharge experiments (Fig. 8b) to 57 cycles in the 15 min experiments (Fig. 8a). Column 5 in Table 3 shows that the average coulombic efficiency of the zinc–cerium battery was below 100% in all the experiments, indicating that the products formed during battery charge did not return completely to their initial states and, therefore, that a secondary reaction likely took place. At long charge times, the Ce(IV) product appeared to accumulate over time without being reduced completely during the discharge phases. This led to a depletion of Ce(III) at the beginning of successive charge phases as the cycle number increased. In all experiments, the life

**Table 3**
Life cycle of a zinc–cerium battery charging at 50 mA cm$^{-2}$ for different lengths of time.

| Charge/discharge cycle time | No. of cycle | Average charge voltage (V) | Average discharge voltage (V) | % Average coulombic efficiency | % Average voltage efficiency | % Average energy efficiency |
|---|---|---|---|---|---|---|
| 0.25 h | 57 | 3.06 | 1.41 | 84.9 | 46.2 | 39.2 |
| 1 h | 19 | 3.00 | 1.75 | 81.5 | 58.3 | 47.5 |
| 2 h | 7 | 2.95 | 1.77 | 69.4 | 60.0 | 41.3 |
| 4 h | 4 | 2.96 | 1.86 | 68.3 | 62.8 | 42.8 |
| First charged for 3 h and then 0.25 h charge/discharge | 25 | 2.97 | 1.77 | 99.4 | 59.6 | 59.3 |

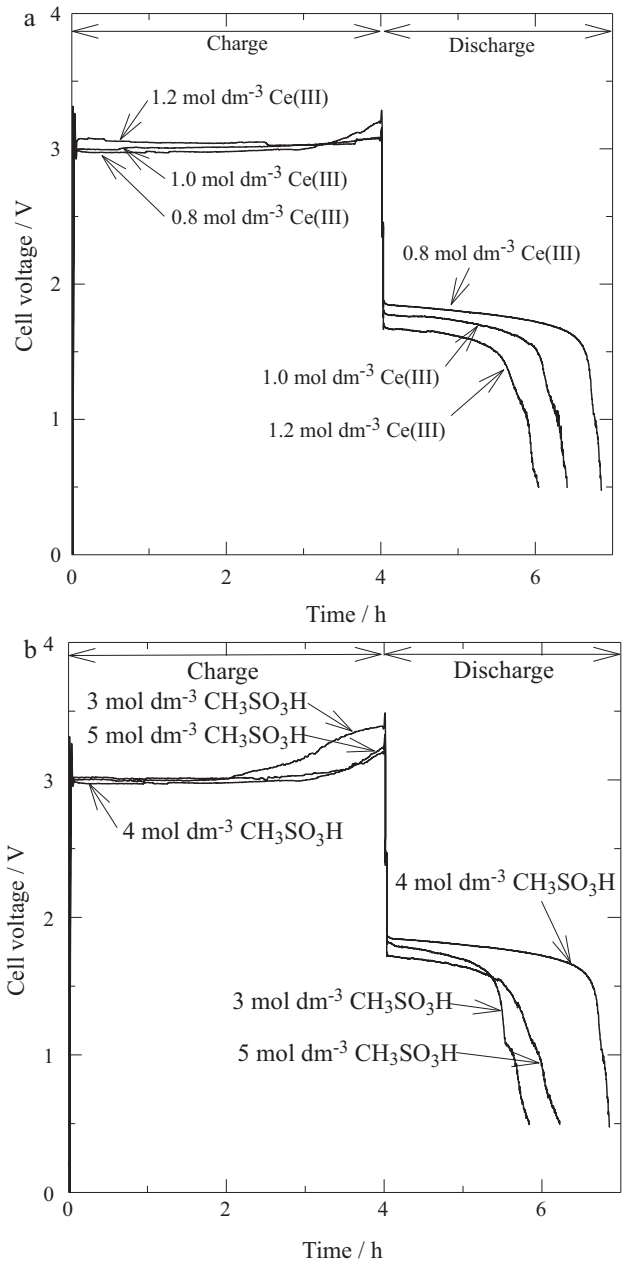


**Fig. 7.** Effect of electrolyte compositions on the charge–discharge performance of a zinc–cerium redox flow battery: (a) cerium (III) concentration and (b) methanesulfonic acid concentration in the positive electrolyte. Unless indicated, electrolyte compositions and operating conditions were the same as in Fig. 3.

of the battery was between 25 and 30 h, except in Fig. 9 where the cell was charged for 3 h before 15 min charge/discharge cycles.

Due to the initial higher acid concentration in the positive compartment and the formation of acid in the negative electrode during battery charge, reaction (1), the acidity of the negative electrolyte increased after prolonged charge/discharge cycling [45], which decreased the efficiency of zinc electrodeposition. For this reason, in all of the long life-cycle experiments, the zinc half-cell reaction was also a limiting factor. The acid concentration change and the diffusion of protons across the membrane were more significant towards the end of the 4 h charge/discharge cycle.

More cycles at longer charge–discharge times can be achieved by increasing the ratio of electrolyte volume to electrode area. As shown in Fig. 8a, the cell voltage during discharge dropped rapidly in the early cycles. The concentration of Ce(IV) ions generated was still too low for the battery to be able to discharge at 50 mA cm$^{-2}$. After a number of cycles, Ce(IV) ions accumulated and higher discharge cell voltages could be obtained. At later cycles, depletion of the Ce(III) led to a sharp increase in charge cell voltages.

In order to achieve long life cycles and a relatively high discharge cell voltage, the battery was first charged at 50 mA cm$^{-2}$ for 3 h to obtain a high concentrations of Ce(IV). Following the 3 h charge, a charge/discharge cycle regime, each 15 min, was applied. This

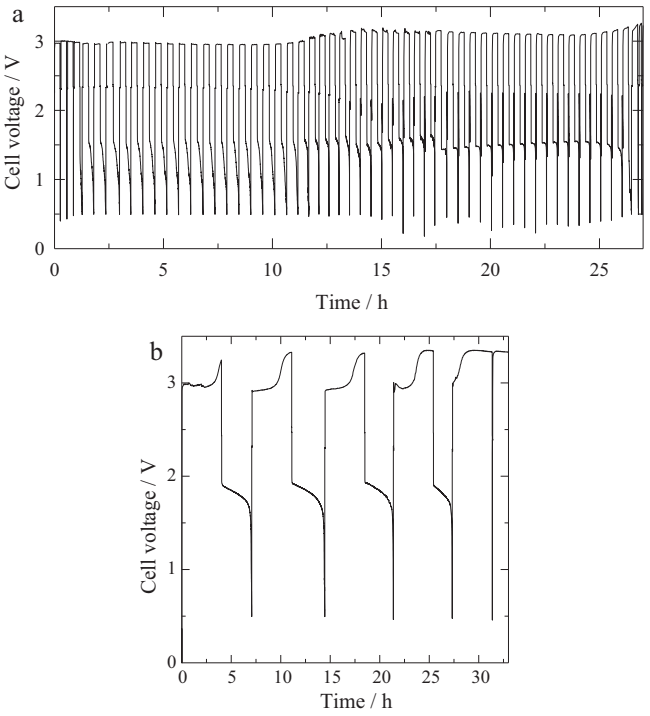


**Fig. 8.** Life cycle of a zinc–cerium battery charging at 50 mA cm$^{-2}$ for different lengths of time: (a) 15 min and (b) 4 h. Electrolyte compositions and operating conditions were the same as in Fig. 3.

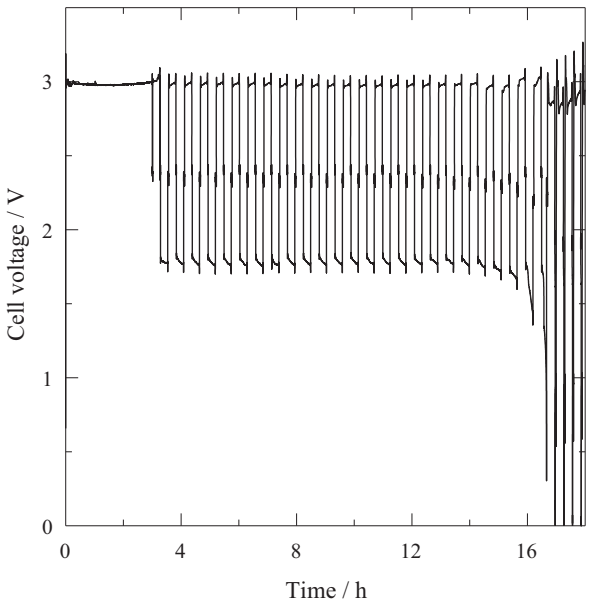


**Fig. 9.** Life cycle of a zinc–cerium battery charging at 50 mA cm$^{-2}$ for 3 h followed by 15 min charge/discharge cycles. Electrolyte compositions and operating conditions were the same as in Fig. 3.

ensured a smaller change in the acid concentration and a slower depletion of Ce(III) ions. Fig. 9 shows that for this experiment, 25 cycles at an average discharge voltage of *c.a.* 1.77 V were obtained with average coulombic and energy efficiencies of 99.4% and 59.3%, respectively, higher than any of the other charge/discharge cycle regimes tested.

## 4. Conclusions

The performance of a zinc–cerium redox flow battery has been characterized through comprehensive investigations into the effects of operating conditions, materials and electrolyte compositions, as well as through life-cycle testing. The two-dimensional electrodes performed poorly. Carbon felt positive electrodes were capable of discharge at 50 mA cm$^{-2}$ with high coulombic (>92%) and voltage (>68%) efficiencies. Due to the poor electrical conductivity and the poor adherence of the carbon adhesive (used to attach the carbon felts) after only a few cycles, a three-dimensional platinised titanium mesh electrode was found to be the optimal positive-electrode material.

The highest energy efficiency was obtained at 50 °C with a mean linear electrolyte flow velocity of 7.8 cm s$^{-1}$, while the optimum composition for the positive electrolyte was 0.8 mol dm$^{-3}$ Ce(III) methanesulfonate in 4.0 mol dm$^{-3}$ methanesulfonic acid. In most cases, flow velocities below 3.9 cm s$^{-1}$ yielded a poor performance. Higher Ce(III) concentrations were not possible as a result of the low solubility in methanesulfonic acid. In all cases, the positive cerium half-cell was limiting for battery discharge due to inefficiencies in the discharge cerium reaction in the early cycles. In all charge/discharge modes at different times, the zinc half-cell reaction was the limiting factor for the life cycles. During the life cycles, the negative electrolyte acidity increased due to the migration of protons from the positive electrolyte and due to proton generation during zinc electrodeposition.

An improved electrolyte composition and alternative electrode materials could be used to enhance the performance of the zinc–cerium redox flow battery. For instance, the use of additives or ionic liquids to reduce secondary reactions such as hydrogen and oxygen, and the use of a catalyst incorporated into the electrode material to enhance the reaction rates. Further investigations into the acid concentrations in the negative and positive electrolytes and the use of bipolar electrodes in a stack, are necessary to scale-up the system and increase the power and energy outputs.

## Acknowledgements

Financial support has been provided by the Research Institute for Industry (RIfI) at the University of Southampton. The authors are grateful to Dr. L. Berlouis, University of Strathclyde for helpful discussions and gratefully acknowledge the construction of the flow battery provided by the mechanical engineering workshop, University of Southampton. This work represents part of P.K. Leung's PhD research programme on the development of zinc-based flow batteries for energy storage and conversion technology.

## References

[1] The Electricity Advisory Committee, Bottling Electricity: Storage as a Strategic Tool for Managing Variability and Capacity Concerns in the Modern grid - A report by The Electricity Advisory Committee, December 2008. http://www.oe.energy.gov/DocumentsandMedia/final-energy-storage_12-16-08.pdf Accessed on 25 November 2010.
[2] N. Tokuda, T. Kanno, T. Hara, T. Shigematsu, Y. Tsutsui, A. Ikeuchi, T. Itou, T. Kumamoto, SEI Tech. Rev. 50 (1998) 88–94.
[3] J. Makansi, J. Abboud, Energy Storage Council White Paper (2002).
[4] M. Yoshitake, M. Takabatake, O. Hamamoto, T. Hiramatu, S. Kondo, J. Proc. Electrochem. Soc. 266 (1988) 11–88.
[5] M. Shimizu, M.S. N. Mori, Japan Patent - 63128560, 01/07/1988, (1988).
[6] A. Pelligri, P.M. Spaziante, GB Patent 2030349, to Oronzio de Nori Impianti Elettrochimici S.p.A., (1978).
[7] M. Skyllas-Kazacos, M. Rychcik, P.G. Robins, A.G. Fane, M.A. Green, J. Electrochem. Soc. 133 (1986) 1057–1058.
[8] M. Rychcik, M. Skyllas-Kazacos, J. Power Sources 19 (1987) 45–54.
[9] M. Skyllas-Kazacos, F. Grossmith, J. Electrochem. Soc. 134 (1987) 2950–2953.
[10] M. Rychcik, M. Skyllas-Kazacos, J. Power Sources 22 (1988) 59–67.
[11] R.F. Koontz, R.D. Lucero, (2000), Handbook of batteries, vol. 39, 1–22.
[12] F.C. Walsh, J. Pure Appl. Chem. 73 (2001) 1819–1837.
[13] DTI, Regenesys Utility Scale Energy Storage, Project Summary, Pub URN 04/1048. http://www.dti.gov.uk/energy/renewables/publications/pubs_distributedgeneration.shtml Accessed on 25 November 2010.
[14] D. Pletcher, R. Wills, J. Power Sources 149 (2005) 96–102.
[15] C. Ponce de León, A. Frías-Ferrer, J. González-García, D.A. Szánto, F.C. Walsh, J. Power Sources 160 (2006) 716–732.
[16] I. Tsuda, K. Kurokawa, K. Nozaki, Conference Record of the Twenty Fourth IEEE Photovoltaic Specialists Conference – 1994, 1994 IEEE First World Conference, vol. 1, 1994, pp. 946–949.
[17] L. Joerissen, J. Garche, C. Fabjan, G. Tomazic, J. Power Sources 127 (2004) 98–104.
[18] K.L. Huang, X.G. Lia, S.Q. Liu, N. Tan, L.Q. Chen, Renewable Energy 33 (2008) 186–192.
[19] R.L. Clarke, B.J. Dougherty, S. Harrison, P.J. Millington, S. Mohanta, US 2004/0202925 A1, Cerium Batteries, (2004).
[20] R.L. Clarke, B.J. Dougherty, S. Harrison, J.P. Millington, S. Mohanta, US 2006/0063065 A1, Battery with bifunctional electrolyte, (2005).
[21] P.K. Leung, C. Ponce de León, C.T.J. Low, F.C. Walsh, submitted to Electrochim. Acta, January 2011.
[22] P.K. Leung, C. Ponce de León, C.T.J. Low, F.C. Walsh, Electrochim. Acta 56 (2011) 2145.
[23] J. Bard, L.R. Faulkner, Electrochemical Methods - Fundamentals and Applications, 2nd ed., Wiley, 2001.
[24] M.D. Gernon, M. Wu, T. Buszta, P. Janney, Green Chem. 1 (1999) 127–140.
[25] R.P. Kreh, R.M. Spotnitz, J.T. Lundquist, J. Org. Chem. 54 (1989) 1526–1531.
[26] T.R. Crompton, Elsevier Science & Technology Books, vol. 14, 3rd ed., Boston: Newnes, Oxford, England, 2000 (vol. Chapter 14).
[27] P.C. Symons, J Electrochem. Soc. International Conference on Electrolytes for Power Sources, Brighton, 1973.
[28] P.C. Butler, P.A. Eidler, P.G. Grimes, S.E. Klassen, R.C. Miles, Handbook of Batteries, vol. 39, 3rd ed., McGraw Hill, 2001.
[29] P.C. Butler, D.W. Miller, A.E. Verardo, 17th Intersoc. Energy Conversion Eng. Conf., Los Angeles (1982).
[30] L.W. Hruska, R.F. Savinell, J. Electrochem. Soc. 128 (1981) 18–25.
[31] Y.H. Wen, J. Cheng, S.Q. Ning, Y.S. Yang, J. Power Sources 188 (2009) 301–307.
[32] B. Fang, S. Iwasa, Y. Wei, T. Arai, M. Kumagai, Electrochim. Acta 47 (2002) 3971–3976.
[33] R.M. Spotnitz, R.P. Kreh, J.T. Lundquist, P.J. Press, J. Appl. Electrochem. 20 (1990) 209–215.
[34] L.B. Zinner, J. Ann. Assoc. Bras. Quim. 30 (1979) 27.
[35] P. Patnaik, Dean's Analytical Chemistry Handbook, 2nd ed., McGraw-Hill, 2004.
[36] I.M. Kolthoff, E.B. Sandell, Texture of Quantitative Inorganic Analysis, 3rd ed. The Macmillan Company, pp. 463–481.

[37] A.I. Vogel, Textbook of Quantitative Inorganic Analysis, 5th ed. Wiley, New York.
[38] V. Devadoss, C.A. Basha, K. Jayaraman, J. Ind. Eng. Chem. Res. 47 (2008) 4607–4616.
[39] H.S. Lim, A.M. Lackner, R.C. Knechtli, J. Electrochem. Soc. 124 (1977) 1154–1157.
[40] A. Pletcher, R. Wills, J. Power Sources 149 (2005) 96–102.
[41] J. Jorné, J.T. Kim, D. Kralik, J. Appl. Electrochem. 9 (1979) 573–579.
[42] Y. Liu, X. Xia, H. Liu, J. Power Sources 130 (2004) 299–305.
[43] T. Raju, C.A. Basha, Chem. Eng. J. 114 (2005) 55–65.
[44] T. Raju, C.A. Basha, J. Ind. Eng. Chem. Res. 47 (2008) 8947–8952.
[45] A. Hazza, D. Pletcher, R. Wills, J. Phys. Chem. Chem. Phys. 6 (2004) 1773–1778.
[46] J.M. Friedrich, C. Ponce-de-León, G.W. Reade, F.C. Walsh, J. Electroanal. Chem. 561 (2004) 203–217.
[47] A.P. Borole, C.Y. Hamilton, T.A. Vishnivetskaya, D. Leak, C. Andras, J. Morrell-Falvey, M. Keller, B. Davison, J. Power Sources 191 (2009) 520–527.
[48] J. Gonzaïlez-Garcıa, P. Bonete, E. Exposito, V. Montiel, A. Aldaz, R. Torregrosa-Macia, J. Mater. Chem. 9 (1999) 419–426.